Quantum Information Processing

Dennis V. Perepelitsa*
MIT Department of Physics
(Dated: April 29, 2007)

We implement a two-qubit quantum computer using bulk-ensemble nuclear magnetic resonance spectroscopy methods. The QC system is described and calibrated. The Deutsch-Jozsa algorithm is successfully executed on every one-bit input boolean function. Grover's algorithm is successfully executed for $N = 40$ iterations on a two-bit search space.

1. INTRODUCTION

Richard Feynman first proposed the idea of performing computations on the quantum scale in 1982, and went on to characterized primitive quantum logic gates three years later.[3] In the decade that followed, a series of theoretical discoveries spurred the interest in practical implementations of quantum computing.

The Deutsch-Jozsa algorithm [1], first presented in 1992, was the first truly *quantum* algorithm in the sense that it took advantage of the quantum nature of its implementation to perform calculations in ways that classical computers could not. Peter Shor followed with a quadratic-time factoring algorithm in 1994, and Lov Grover [2] presented a fast database search algorithm in 1996.

In 1997, Gershenfeld et. al. and Cory et. al. proposed nuclear magnetic resonance implementations of a quantum computer, using spin eigenstates of entangled particles as qubits and standard NMR pulses as state operators. This is the implementation used by our system.

2. THEORY

The system we describe has two distinct nuclear spins, organized by the size of their magnetic moment, which serve as the computational basis, listed below.

$$\{|00\rangle, |01\rangle, |10\rangle, |11\rangle\} = \{|\uparrow\downarrow\rangle, |\uparrow\downarrow\rangle, |\downarrow\uparrow\rangle, |\downarrow\downarrow\rangle\} \quad (1)$$

At any time, the system is described by the tensor product of two state vectors in the Bloch sphere representation. By applying transverse radiofrequency pulses of a frequency close to that of the desired qubit, we can perform rotations of either state vector.

$$R_x = \frac{1}{\sqrt{2}}\begin{bmatrix} 1 & -i \\ -i & 1 \end{bmatrix}, \; R_y = \frac{1}{\sqrt{2}}\begin{bmatrix} 1 & -1 \\ 1 & 1 \end{bmatrix} \quad (2)$$

We include an index after x or y to indicate which qubit the rotation is acting on. Strictly speaking, an operation O on the first qubit should be written as the tensor product $[O_1 \otimes I_2]$, but we drop this when the meaning is clear.

TABLE I: Classification of Deutsch-Jozsa functions

Function	Action on $(0,1)$	U_f	DJ Result
f_1: ZERO	$(0,0)$	I	$\|00\rangle$
f_2: ONE	$(1,1)$	R_{x1}^2	$-\|00\rangle$
f_3: ID	$(0,1)$	U_{CNOT}	$\|10\rangle$
f_4: NOT	$(1,0)$	$R_{x1}^2 U_{CNOT}$	$-\|10\rangle$

When no pulses are applied to induce rotations, the Hamiltonian contains a free-evolution term that comes from first-order *spin-spin coupling* of the nuclei. If the system is allowed to evolve freely for a time $T = 1/(2J)$ where J is a physical property of the system known as the coupling constant, the system will undergo a transformation we define by τ. It is this evolution that accounts for the entanglement of the particles, and gives the system a component that is not classically replicable.

$$\tau = \exp\left[\frac{i\pi}{2} JT \sigma_{z1} \otimes \sigma_{z2}\right] = e^{i\pi/4} \, \mathrm{diag}(-i, 1, 1, -i) \quad (3)$$

For a given boolean function f with one boolean input, we define the corresponding unitary operator U_f by the action of f, as follows.

$$U_f \, |x \; y\rangle = |x \; (f(x) \oplus y)\rangle \quad (4)$$

The $\oplus$ operation above is addition modulo 2, also known as XOR. A particularly key operator, called the *controlled-not* logic gate is implemented below with a series of rotations and a free evolution. Feynman [3] offers an excellent overview of quantum logic gates.

$$U_{CNOT} \, |x \; y\rangle = |x \; (x \oplus y)\rangle \quad (5)$$

$$U_{CNOT} = R_{y1}^{-1} \tau R_{y1} R_{x1} R_{x2} R_{y2} R_{x2}^{-1} \quad (6)$$

We turn to the problem of initial state preparation. The Boltzmann distribution dictates that due to the differences in the energy eigenvalues, the system is not quite at a pure mixture of the four states. The thermal density matrix ρ_{therm} is roughly equal to

*Electronic address: dvp@mit.edu

$$\rho_{therm} \approx \frac{1}{4} I + 10^{-4} \text{ diag}(5, 3, -3, -5) \tag{7}$$

We refer to this state as the *thermal state* and use it later for calibration purposes. It is undesirable, since many quantum algorithms require the specific pure initial state $|00\rangle$. We get around this by using a *time-averaging* method to create a *pseudopure* state. It works by cyclically permuting the last three elements along the diagonal with rotations and then averaging the result of the desired pulse sequence from all permutations, and taking the average. It can be shown that this average gives the same result as if the pulse sequences acted only on the pure state $|00\rangle$. A more detailed description is provided in the lab guide [4].

2.1. Deutsch-Jozsa Algorithm

We present here a simplified version of the algorithm devised by Deutsch and Jozsa [1] (extensions to functions with more bits of inputs are straightforward). Let f be a function with 1 bit of input and 1 bit of output, implemented with the operator U_f, as described above. We characterize all such f in Table I. Classically, we would have to evaluate $f(0)$ and $f(1)$ to determine if both outputs are represented. However, consider the action of the following pulse sequence on the pure state $|00\rangle$.

$$(R_{y2}^{-1} R_{y1}) U_f (R_{y2} R_{y1}^{-1}) |00\rangle = \tag{8}$$
$$\frac{1}{2}\left[(-1)^{f(0)}(|0\rangle - |1\rangle) + (-1)^{f(1)}(|0\rangle + |1\rangle)\right] \otimes |0\rangle$$

If both 0 and 1 are outputs, the result of (8) is $|10\rangle$. Otherwise, it is $|00\rangle$. By measuring the system a single time, we can determine whether one of $(f1, f2)$ or $(f3, f4)$ is present.

2.2. Grover's Algorithm

Let f be a boolean function with two bits of input which returns true ($f = 1$) for exactly one input x_0. Grover's database search algorithm [2] determines this input with only a single observation. We present it here with a search space of four basis states.

Pick the "needle in the haystack" basis state x_0. Define O as the operator that flips the sign of this state and leaves all others unperturbed. Called the *Oracle*, this operator distinguishes x_0 from the other states in a straightforward manner. Though we implement the Oracle directly with a pulse sequence, it must be noted that the action of the operator could arise from some other mechanism and need not be known to the experimenter. Next, define the *Hadamard* operator H as

TABLE II: Pulse implementation of Grover's algorithm operators

$G(x_0 = \|00\rangle)$	$R_{x1}^{-1} R_{y1} R_{x2}^{-1} R_{y2} \tau R_{x1}^{-1} R_{y1} R_{x2}^{-1} R_{y2}$
$G(x_1 = \|01\rangle)$	$R_{x1}^{-1} R_{y1} R_{x2}^{-1} R_{y2} \tau R_{x1}^{-1} R_{y1} R_{x2} R_{y2}$
$G(x_2 = \|10\rangle)$	$R_{x1}^{-1} R_{y1} R_{x2}^{-1} R_{y2} \tau R_{x1} R_{y1} R_{x2}^{-1} R_{y2}$
$G(x_3 = \|11\rangle)$	$R_{x1}^{-1} R_{y1} R_{x2}^{-1} R_{y2} \tau R_{x1} R_{y1} R_{x2} R_{y2}$

$$H = \frac{1}{\sqrt{2}} \begin{bmatrix} 1 & 1 \\ 1 & -1 \end{bmatrix} \otimes \frac{1}{\sqrt{2}} \begin{bmatrix} 1 & 1 \\ 1 & -1 \end{bmatrix} \tag{9}$$

Finally, let the phase-shift operator $P = \text{diag}(1, -1, -1, -1)$. The composite Grover operator $G = HPHO$ is the heart of the algorithm, as we will see. Table II gives the rf pulse realization of the operator G for each choice of x_0.

Obtain the maximally mixed state by applying H to $|00\rangle$. Every iteration of G rotates the state vector by 60° through the $(H|00\rangle \times |x_0\rangle)$ plane. Thus, after only a single iteration, the system is in the selected state. Every additional $N = 3$ applications of G returns the system to state $|x_0\rangle$. The single-evaluation search, and the oscillatory nature are principal features of this quantum algorithm. Chuang and Nielsen [5] have an intuitive geometric visualization of this process, as well as a more in-depth description.

3. EXPERIMENTAL SETUP

The data acquisition system consists of a Bruker Avance 200 NMR spectrometer and two control computers, as pictured in Figure 1. A workstation issues commands over the network through a MATLAB interface to another machine running Bruker NMR software, which transmits and receives NMR pulse information from the spectrometer. A more detailed description of the software involved is available in the lab guide [4].

The NMR sample is a sealed vial of $^{13}CHCl_3$ placed in a strong superconducting magnet, which is then spun rapidly to average out inhomogeneities in the field. The sample sits surrounded by coils in the transverse plane which are used as the circuity for both delivering radiofrequency pulses to the sample as well as collecting the induced signal from the precessing nuclei. The transmission chain and signal collection circuitry are tuned to operate at the resonant frequency of the proton and carbon-13. Tqhe spin of carbon nucleus and proton, respectively, are the first and second qubit in our system.

The pulse reception chain amplifies and filters the free induction decay signal, which is then Fourier transformed into the frequency domain by the software, resulting in two roughly Lorentzian lineshapes. The measured voltage is complex-valued since the superheterodyne receiver

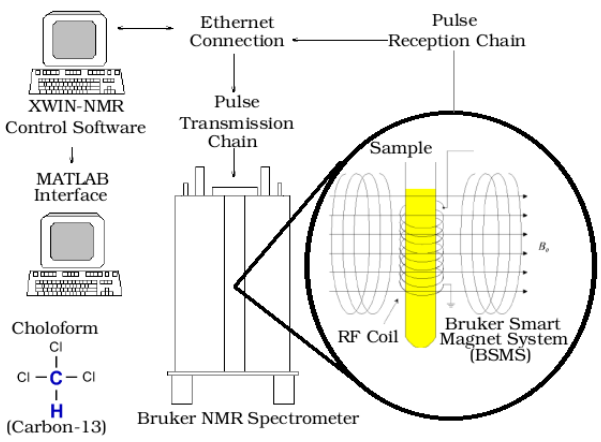

FIG. 1: Schematic of the Bruker acquisition system.

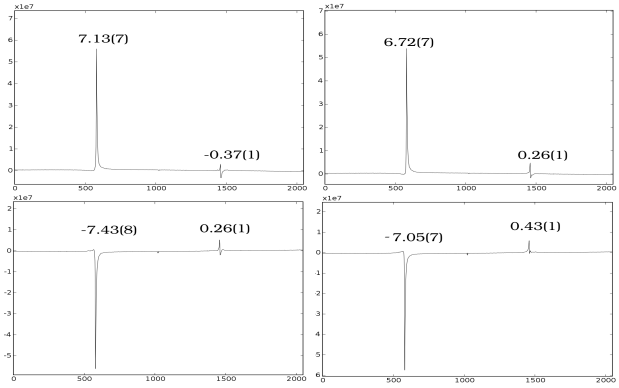

FIG. 2: Proton spectra of the result of the Deutsch-Jozsa algorithm. Left to right, top to bottom, the functions are f_1, f_2, f_3 and f_4. Frequency is on the abscissa, voltage is on the ordinate. The peaks are labeled with their normalized value.

in the pulse reception chain is capable of distinguishing the direction of precession as well as its frequency.

To actually observe signal, we rotate the state vector along the x-axis into the plane of the rf coil with a 90° readout pulse. For a diagonal density matrix $\rho = \mathrm{diag}(a, b, c, d)$, the left and right proton and left and right carbon peaks are $(a-c)$, $(b-d)$, $(a-b)$ and $(c-d)$, respectively. The laboratory guide [4] explains in more detail how the proton and carbon spectra arise from the density matrix after the application of the readout operator.

4. ERROR ANALYSIS

All readout spectra exhibited a level of background noise. The average of this noise was subtracted from the numerically integrated value of the peaks, and its standard deviation was taken to be the uncertainty in the contribution from any individual point. In most cases, asymmetries in the observed lineshape and insufficient amount of uncertainty made fitting to a Lorentzian profile impossible. Numerical integration using Simpson's rule and this source of background fluctuation provided peak integrals with uncertainty on the order of .5%.

While processing the Deutsch-Jozsa data, the absolute value of the signal was integrated, since no phase differences were expected. While processing the Grover data, both real and imaginary parts were integrated, since phase played an important role. The exception to numerical integration was the case of a few thermal state spectra, which we were able to fit to Lorentzian lineshapes using standard non-linear fitting methods. These spectra provide for some of the system parameters descibed above.

A quantitative measure of random error was obtained by taking twenty spectra of the thermal state and comparing the integrated peak values. The relative random error was on the order of 1%. At the beginning of each day, a calibration spectrum of the thermal state was taken, and the calculated values set to the reference $(8, 8)$ and $(2, 2)$ for the proton and carbon spectra, respectively, by design.

Observed peak integrals were then normalized using that day's calibration peak integrals. The random error and both background fluctuation uncertainties were added in quadrature to obtain the final peak integral uncertainty.

5. RESULTS

5.1. System parameters

We used several methods to determine fundamental parameters of our QC system. Using the fluctuations in the noise of the Fourier spectrum as a source of uncertainty, we were able to perform least-squares fits of Lorentzian lineshapes to the proton and carbon readouts of the thermal state. The pairs of peaks were centered at $\omega_p = 200.13$MHz and $\omega_c = 50.33$MHz, respectively, with accuracy to that many digits. The separation between them in frequency space is the *spin-spin coupling constant* $J = 214.99(1)$Hz. The full-width half-maximum of the peaks is the inverse of the spin-spin relaxation time. Averaging the values obtained across the spectra, and using standard error propagation methods presented in Bevington [6], we obtain $T_2 = 1.21(1)$s. The lowest χ^2_ν obtained for these fits was 11.1.

Using a standard inversion recovery method implemented with a $90° - T - 180°$ pulse sequence, we plotted peak height against 60 delay times T, and obtained an exponential fit. The resulting spin-lattice relaxation time was found to be $T_1 = 21.8(1)$s. Then, we plotted the net magnetization against 60 values of varying pulse widths and obtained a damped sinusoidal fit. The first maxima on the plot were taken to be the 90° pulse widths, with $pw_p = 9.2$ms and $pw_c = 8.4$ms, respectively. χ^2_ν for these fits ranged in the high single digits.

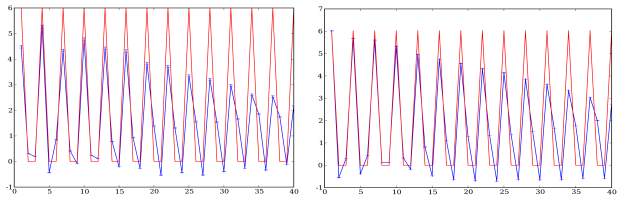

FIG. 3: Relevant peak heights plotted over forty iterations of Grover's algorithm with $x_0 = |00\rangle$. Left to right, these are the left proton and right carbon peak. Iterations of Grover's algorithm is on the abscissa, normalized peak height is on the ordinate. The red line is the predicted value, and the blue line is the result of the experiment.

5.2. Deutsch-Jozsa algorithm

Figure 2 displays the resultant proton readout spectra for the result of applying the Deutsch-Jozsa algorithm with each of the four functions. The top two spectra clearly correspond to $|00\rangle$ and the bottom two to $|10\rangle$. As expected, a single observation is enough to distinguish the "fair coin" functions from the others.

The left and right peaks are within a $15-20\%$ deviation from the expected values of $(6,0)$ for the top two spectra and $(-6,0)$ for the bottom two, respectively. The carbon spectra, which we do not show for lack of space, showed a slightly better agreement with theory, the left and right peaks exhibiting a 10% deviation from the expected values of $(6,0)$ and $(0,6)$.

5.3. Grover's algorithm

Although we were successful in obtaining similar data for all four possible implementations of Grover's algorithm, we present here only the $x_0 = |00\rangle$ results. Figure 3 presents two key peaks in the carbon and proton spectra. These peaks are the left proton and right carbon peaks, and both should be 6.0 after normalization when the system is in the state x_0. We can see that not only is this state entered after only one iteration of the algorithm, but that it repeats at $N = 4, 7, 10, \ldots$, as predicted, confirming the oscillatory nature of this quantum algorithm.

The net magnetization seems to decay over time, but this is far from surprising. Each iteration of Grover's algorithm consists of eight rf pulses and two free-evolution decays. The length of forty iterations of this pulse sequence begins to rival the spin-spin relaxation time of the system T_2. The magnetization fall-off can thus be attributed to the system slowly relaxing to equilibrium.

6. CONCLUSION

We have implemented two quantum algorithms with no classical analogue on a two-qubit quantum computer using NMR spectroscopy methods. The fact that our system calibration produced fits with high values of the χ^2_ν parameter is more an artifact of the lack of significant random error, and of imperfections in the observed lineshape.

We have successfully executed the Deutsch-Jozsa algorithm on all one-bit input boolean functions, with deviation no more than 15% on the average from the expected peak integrals. We have successfully executed Grover's searching algorithm with $N = 40$ iterations on every possible value of x_0, and have confirmed the oscillatory nature of the algorithm. Without significant improvement to our estimation of systematic error or experiment technology, we believe this number of iterations is close to the maximum before system decoherence trumps the observed signal.

While our experimental setup gives strong qualitative agreement with the expected results, our calculated uncertainty is not nearly enough to cover the deviations of the observed peak integrals from their predicted value. There are a number of sources of systematic error which could account for this. The observed asymmetric lineshapes present in our frequency spectra could have arisen from improper even-order shimming of the magnet. Systematic inhomogeneities are no doubt present in the magnetic field or the rf coils, and imperfect pulse widths would lead to a deterioration of the system over time.

The presence and order of these systematics is a topic for further investigation.

[1] D. Deutsch and R. Jozsa, Proc. Royal Soc. London **A439** (1992).

[2] L. Grover, Proc. 28th ACM symposium on Theory of computing (1996).

[3] R. P. Feynman, Optics News (1985).

[4] J. L. Staff, *Quantum information processing*, URL `http://web.mit.edu/8.13/www/JLExperiments/JLExp49.pdf`.

[5] I. Chuang and M.A.Nielsen, *Quantum Computation and Quantum Information* (Cambridge University Press, 2000).

[6] P. Bevington and D. Robinson, *Data Reduction and Error Analysis for the Physical Sciences* (McGraw-Hill, 2003).

Acknowledgments

DVP gratefully acknowledges Brian Pepper's equal partnership, as well as the guidance and advice of Thomas Walker, Daniel Nezich and Scott Sewell.